JASA ARTICLE

Insertion loss of a thin partition for audio sounds generated by a parametric array loudspeaker

Jiaxin Zhong,[a] Shuping Wang, Ray Kirby,[b] and Xiaojun Qiu[c]
Centre for Audio, Acoustics and Vibration, Faculty of Engineering and Information Technology, University of Technology Sydney, Sydney, New South Wales 2007, Australia

ABSTRACT:
Unlike the audio sound generated by traditional sources, the directivity of that generated by a parametric array loudspeaker (PAL) deteriorates significantly after passing through a thin partition. To study this phenomenon, the PAL radiation model based on the Westervelt equation, and the plane wave expansion method are used to calculate the sound fields behind a sheet of aluminum foil and a porous material blanket under the quasi-linear assumption, where the paraxial approximation is assumed only for ultrasonic waves. The audio sounds generated by a point monopole and a traditional directional source are presented for comparison. Both simulation and experiment results show that the transmitted sound from a PAL behind the thin partition is small and less focused on the radiation axis because most of the ultrasounds forming the directivity of the PAL is blocked by the thin partition which has little effect on the traditional audio sources. © *2020 Acoustical Society of America*. https://doi.org/10.1121/10.0001568

(Received 28 January 2020; revised 16 June 2020; accepted 23 June 2020; published online 14 July 2020)
[Editor: Andi Petculescu] Pages: 226–235

I. INTRODUCTION

Parametric acoustic arrays (PAAs) have attracted much attention due to their capability of generating highly directional sound beams at low frequencies.[1] Parametric array loudspeakers (PALS) are an application of the PAAs for radiating highly directional audio sounds in air with the carrier wave of ultrasounds.[2,3] It is found in experiments the directivity of audio sounds generated by a PAL deteriorates significantly after introducing a thin and homogeneous partition. Existing analytical models of PALS consider the sound radiation in free field but pay little attention to its transmission through a partition.

Understanding the insertion loss of the partition for audio sounds generated by a PAL is important in applications. For example, with the capability of producing quasi-plane waves, PALS can be used to measure the acoustic parameters of materials *in situ* by measuring the sound pressure on the transmission side of the specimen.[4] The sharp directivity of PALS is attractive to mobile phone designers.[5] However, the size of the effective radiation surface should be as large as possible to generate considerable sound levels. A natural way is to install a PAL under the phone screen, so the effects of the thin screen on the generated audio sound need to be known. In research, one may need a circular PAL in experiments for verifying the analytical model, but there are only square/rectangular commercial PALS. It is shown in Secs. III and IV of this paper that a circular PAL can be constructed by covering a square one with a 6 mm thick Perspex panel.

The thin partition considered in this paper implies that the thickness of the partition is small compared with the audio wavelength and the effective absorption length of the PAL. The transmission of an audio plane wave through a thin partition is well known and the mass law is widely used to predict the insertion loss.[6] The effects of a thin partition on spherical waves radiated by a point monopole were also studied where the transmission loss and the insertion loss are derived analytically using the plane wave expansion method.[7] The transmission of a diffuse incident sound through a partition has also been well studied.[8] However, there is little research reported on the transmission of audio sounds generated by a PAL through a thin partition.

When a PAL radiates two intensive ultrasound (primary) waves with different frequencies, a secondary wave containing the difference-frequency wave (the audio sound in air) is generated due to the nonlinearity. The most widely used Khokhlov–Zabolotskaya–Kuznetsov (KZK) equation considers the diffraction, absorption and nonlinearity of this phenomenon under the parabolic approximation, and many methods have been proposed to solve the KZK equation analytically or numerically; but the results are usually only valid within the paraxial region about 20° from the transducer axis.[9] If the paraxial approximation is not assumed for audio waves, the non-paraxial model can be used to predict the sound at wide angles.[10,11] Later on, a spherical expansion method is proposed to simplify the calculations.[12] However, there is currently no analytical model for calculating the transmission of the sound field generated by a PAL through a partition. It is developed

[a]Electronic mail: Jiaxin.Zhong@student.uts.edu.au, ORCID: 0000-0002-9972-8004.
[b]ORCID: 0000-0002-3520-1377.
[c]ORCID: 0000-0002-5181-1220.

https://doi.org/10.1121/10.0001568

under the quasi-linear assumption in this paper based on the non-paraxial model used for PALs and the plane wave expansion method.

II. THEORY

A sketch of a PAL radiating sound through a partition is shown in Fig. 1, where the radiation axis of the PAL is perpendicular to the partition surface for simplicity. The density and the sound speed in air are ρ_0 and c_0, respectively. A rectangular coordinate system O-xyz is established where the origin, O, is at the projection of the center of the PAL on the partition surface and the z-axis is perpendicular to the surface. The center of PAL is at $(0, 0, z_P)$ where $z_P < 0$. The thickness of the infinitely large partition is assumed to be small enough compared with the audio wavelength and the effective absorption length of the PAL for simplicity. The partition is placed at $z = 0$ and its area density is M.

When ultrasounds at two different frequencies f_1 and f_2 ($f_1 > f_2$) are radiated by the PAL, infinitely many virtual audio sources with the frequency $f_a = f_1 - f_2$ are formed everywhere as long as there exist ultrasounds under the quasilinear assumption.[11] When the ultrasounds are incident on the partition, there are reflected and transmitted ultrasounds with respect to the partition and they produce new virtual audio sources on the incident ($z < 0$) and transmission ($z > 0$) sides, respectively. The audio sounds generated by the ultrasounds inside the partition are very small, so they are neglected in this paper.

The audio sounds generated by these three kinds of virtual audio sources, i.e., those generated by incident, reflected, and transmitted ultrasounds, all propagate through the partition and there are consequently reflected and transmitted audio sounds. In this paper, only the audio sounds on the transmission side ($z > 0$) are considered for calculating the insertion loss of the partition. Based on the above analysis, there are four audio sound components on the transmission side: the transmitted audio sound generated by the incident and reflected ultrasounds, the audio sound generated by the transmitted ultrasound and its reflection on the transmission side.

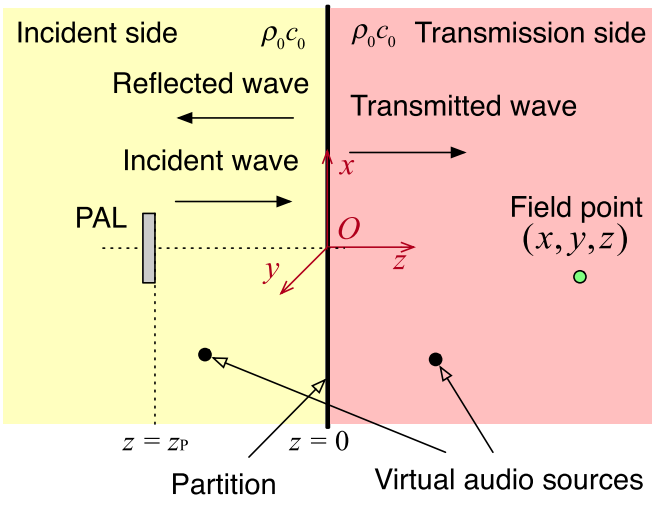

FIG. 1. (Color online) Sketch of a PAL near a thin partition.

Because the audio sound generated by the reflected ultrasound radiates in the direction which is away from the partition toward the PAL source direction, the transmitted sound of these audio sounds is small and can be neglected. Similarly, the reflection of the audio sound generated by the transmitted ultrasound can be neglected as well. Therefore, two audio sound components dominate the sound field on the transmission side, so the total sound pressure of audio sounds can be expressed approximately as

$$p_{a,tot}(\mathbf{r}) = p_{a,inc}(\mathbf{r}) + p_{a,tr}(\mathbf{r}), \quad z > 0, \tag{1}$$

where $p_{a,inc}(\mathbf{r})$ and $p_{a,tr}(\mathbf{r})$ represent the transmitted sound of the audio sound generated by incident ultrasounds and the audio sound generated by transmitted ultrasounds, respectively.

A. Transmission of audio sounds generated by incident ultrasounds

The incident ultrasounds can be calculated by the Rayleigh integral as[10,11]

$$p_{n,inc}(\mathbf{r}) = -\frac{j\rho_0\omega_n v_0}{2\pi}\iint_S \frac{e^{-\alpha_n d_P + jk_n d_P}}{d_P} dx_P dy_P, \quad z_P < z < 0, \tag{2}$$

where the time dependence $e^{-j\omega_n t}$ is omitted, j is the imaginary unit, and the PAL is assumed to be driven by a baffled piston with the velocity amplitude v_0 for both ultrasonic waves over the surface S. The wavenumber $k_n = \omega_n/c_0$, $n = 1$ and 2, $\omega_n = 2\pi f_n$, α_n is the sound attenuation coefficient of the ultrasound in air at the frequency f_n,[13,14] and $d_P = \sqrt{(x - x_P)^2 + (y - y_P)^2 + (z - z_P)^2}$ is the distance between the field point $\mathbf{r} = (x, y, z)$ and the source point $\mathbf{r}_P = (x_P, y_P, z_P)$ on the PAL surface.

The transmitted sound of the audio sound generated by incident ultrasounds at the field point $\mathbf{r}$ on the incident side can be expressed as[10,11]

$$p_{a,inc}(\mathbf{r}) = -\frac{j\rho_0\omega_a}{4\pi}\int_{z_P}^{0}\int_{-\infty}^{\infty}\int_{-\infty}^{\infty} q_{inc}(\mathbf{r}_v) \times \frac{e^{-\alpha_a d_v + jk_a d_v}}{d_v} dx_v dy_v dz_v, \quad z_P < z < 0, \tag{3}$$

where the source density function at the virtual source point $\mathbf{r}_v$ is

$$q_{inc}(\mathbf{r}_v) = -\frac{j\beta\omega_a}{\rho_0^2 c_0^4} p_{1,inc}(\mathbf{r}_v) p^*_{2,inc}(\mathbf{r}_v), \quad z_P < z_v < 0, \tag{4}$$

β is the nonlinearity coefficient, $\omega_a = 2\pi f_a$ is the angular frequency at the audio frequency f_a, the wavenumber $k_a = \omega_a/c_0$, α_a is the sound attenuation coefficient of the

audio sound in air at the frequency f_a, and $d_v = \sqrt{(x-x_v)^2+(y-y_v)^2+(z-z_v)^2}$ is the distance between field point $\mathbf{r}$ and virtual source point $\mathbf{r}_v$. It should be noted that Eq. (3) is derived based on the Westervelt equation, where the Lagrangian density characterizing the local effects is neglected.[15,16] Further simulations (not shown in this paper for conciseness) verify that the error is less than 0.2 dB when the distance between the field point and the PAL is larger than 0.3 m for the parameters used in this paper, which indicates that the method is sufficiently accurate for the model investigated.

The transmitted sound of the audio sound generated by incident ultrasounds can be calculated by using the plane wave expansion (Sec. 26 in Ref. 17 or Chap. 2 in Ref. 18). For a point monopole located at $\mathbf{r}_m = (x_m, y_m, z_m)$ with a source strength of Q_m, the transmitted sound at field point $\mathbf{r}$ on the transmission side of the partition can be expressed as[7]

$$p_{m,tr}(\mathbf{r}) = -\frac{j\rho_0\omega_a Q_m}{4\pi}K(\mathbf{r},\mathbf{r}_m), \quad z>0, z_m<0, \tag{5}$$

where the Weyl's integral [Eq. (2.64) in Ref. 18]

$$K(\mathbf{r},\mathbf{r}_m) = \frac{j}{2\pi}\int_{-\infty}^{\infty}\int_{-\infty}^{\infty}\frac{T_p}{k_{a,z}}e^{j\left[k_x(x-x_m)+k_y(y-y_m)+k_{a,z}|z-z_m|\right]}dk_x dk_y. \tag{6}$$

In Eq. (6), $k_{a,z} = \sqrt{(k_a+j\alpha_a)^2-k_\rho^2}$, $k_\rho^2 = k_x^2+k_y^2$, and the unit of $K(\mathbf{r}, \mathbf{r}_m)$ is the same as the wavenumber. T_p is the sound pressure transmission coefficient for the plane wave with the wavevector $\mathbf{k}_a = (k_x, k_y, k_{a,z})$ (Sec. 3.8 in Ref. 6)

$$T_p = \frac{2\rho_0\omega_a/k_{a,z}}{-j\omega_a M+2\rho_0\omega_a/k_{a,z}}. \tag{7}$$

If the thin partition is porous material, the flow resistance is taken into account and the sound pressure transmission coefficient is modified as (Sec. 3.8 in Ref. 6)

$$T_p = \frac{2\rho_0\omega_a/k_{a,z}}{[-1/(j\omega_a M)+1/R_f]^{-1}+2\rho_0\omega_a/k_{a,z}}, \tag{8}$$

provided that the material is homogeneous, where R_f is the specific flow resistance.

With the above expressions, the transmitted sound of the audio sound generated by incident ultrasounds on the transmission side in Eq. (3) is expressed as

$$p_{a,inc}(\mathbf{r}) = -\frac{j\rho_0\omega_a}{4\pi}\int_{z_P}^{0}\int_{-\infty}^{\infty}\int_{-\infty}^{\infty}q_{inc}(\mathbf{r}_v)K(\mathbf{r},\mathbf{r}_v)dx_v dy_v dz_v, \quad z>0. \tag{9}$$

It is worth noting that Eq. (6) is hard to converge because the small sound attenuation coefficient at the audio frequency makes the integrand singular at $k_{a,z} = \sqrt{(k_a+j\alpha_a)^2-k_\rho^2} \approx 0$ when $k_\rho = k_a$. By using the variable substitution and the integral representation for the Bessel function at order zero $J_0(x) = \pi^{-1}\int_0^\pi e^{jx\cos\theta}d\theta$, Eq. (6) can be reduced to

$$\begin{aligned}K(\mathbf{r},\mathbf{r}_v) = {} & j\int_0^{\pi/2}T_p k_a^2 J_0(k_a\rho_v\cos\gamma)e^{j\sqrt{(k_a+j\alpha_a)^2-k_a^2\cos^2\gamma}|z-z_v|}\\ & \times\frac{\sin\gamma\cos\gamma}{\sqrt{(k_a+j\alpha_a)^2-k_a^2\cos^2\gamma}}d\gamma\\ & +\int_0^{\infty}T_p k_a^2 J_0(k_a\rho_v\cosh\gamma)e^{-\sqrt{k_a^2\cosh^2\gamma-(k_a+j\alpha_a)^2}|z-z_v|}\\ & \times\frac{\sinh\gamma\cosh\gamma}{\sqrt{k_a^2\cosh^2\gamma-(k_a+j\alpha_a)^2}}d\gamma,\end{aligned} \tag{10}$$

where $\rho_v = \sqrt{(x-x_v)^2+(y-y_v)^2}$ is the transverse distance between the field point and the virtual source point, both integrals on the right-hand side are numerically calculated by the 1/3 Simpson rule in this paper, and the dummy variable of the second integral, γ, is replaced by $\tan[(\gamma+1)\pi/4]$ to transform the infinitely large interval into a finite one.

B. Audio sounds generated by transmitted ultrasounds

Because it is hard to apply the plane wave expansion directly on the incident ultrasounds, the Gaussian beam expansion (GBE) method is used in this paper to simplify the Rayleigh integral Eq. (2) into a finite summation.[19] Although the GBE method assumes the paraxial approximation for the ultrasonic waves, further simulations (not shown in this paper for conciseness) without the paraxial approximation using the parameters in this paper verify that the calculation errors for the audio sounds are less than 0.4 dB at the positions on the transmission side. When the PAL is driven by a circular piston with the radius of a, Eq. (2) can be expanded into the superposition of Gaussian beams as[10,12]

$$\begin{aligned}p_{n,inc}(\mathbf{r}) = {} & \sum_{l=1}^{L}\frac{\rho_0 c_0 v_0 A_l}{1+jB_l z/R_n}\\ & \times e^{\left[-B_l/(1+jB_l z/R_n)\right]\left[(x^2/a^2)+(y^2/a^2)\right]+j(k_n+j\alpha_n)(z-z_P)},\\ & z_P<z<0,\end{aligned} \tag{11}$$

where $R_n = (k_n+j\alpha_n)a^2/2$, $n=1, 2$, A_l and B_l are the Gaussian beam coefficients which are determined by the velocity profile of the transducer, and L is the Gaussian beam number. For the circular piston source in this paper, the expansion coefficients have been calculated based on the optimization theory for $L=10$,[19] $L=15$,[20] $L=25$,[21] or $L=40$,[22] where larger L provides more accurate results.

The ultrasound can be expanded into plane waves using the plane wave expansion method to give

https://doi.org/10.1121/10.0001568

$$p_{n,\mathrm{inc}}(\mathbf{r}) = \frac{\rho_0 c_0 v_0 a^2}{4\pi}\sum_{l=1}^{L}\frac{A_l}{B_l} \times \int_{-\infty}^{\infty}\int_{-\infty}^{\infty} \mathrm{e}^{-\left[(k_x^2+k_y^2)/4B_l\right]a^2+\mathrm{j}[k_x x+k_y y+k_{n,z}(z-z_\mathrm{P})]}\mathrm{d}k_x\mathrm{d}k_y, \quad z_\mathrm{P} < z < 0, \tag{12}$$

where $n = 1, 2$ and $k_{n,z} = \sqrt{k_n^2 - k_\rho^2}$. Similar to Eq. (6), the transmitted ultrasound can be obtained as

$$p_{n,\mathrm{tr}}(\mathbf{r}) = \frac{\rho_0 c_0 v_0 a^2}{2}\sum_{l=1}^{L}\frac{A_l}{B_l}\int_0^{\infty} T_\mathrm{p}\mathrm{J}_0(k_\rho\rho)k_\rho \times \mathrm{e}^{-(k_\rho^2 a^2/4B_l)+\mathrm{j}k_{n,z}(z-z_\mathrm{P})}\mathrm{d}k_\rho, \quad z > 0, \tag{13}$$

where T_p is the sound pressure transmission coefficient for a plane wave with the wavevector $\mathbf{k}_n = (k_x, k_y, k_{n,z})$, $\rho = \sqrt{x^2+y^2}$, and the integral on the right-hand side is numerically calculated by the 1/3 Simpson rule in this paper.

The audio sounds generated by transmitted ultrasounds on the transmission side can be expressed as

$$p_{\mathrm{a,tr}}(\mathbf{r}) = -\frac{\mathrm{j}\rho_0\omega_\mathrm{a}}{4\pi}\int_0^{\infty}\int_{-\infty}^{\infty}\int_{-\infty}^{\infty} q_\mathrm{tr}(\mathbf{r}_\mathrm{v})\frac{\mathrm{e}^{-\alpha_\mathrm{a}d_\mathrm{v}+\mathrm{j}k_\mathrm{a}d_\mathrm{v}}}{d_\mathrm{v}} \times \mathrm{d}x_\mathrm{v}\mathrm{d}y_\mathrm{v}\mathrm{d}z_\mathrm{v}, \quad z > 0, \tag{14}$$

where the source density function of the virtual audio source at $\mathbf{r}_\mathrm{v}$ is

$$q_\mathrm{tr}(\mathbf{r}_\mathrm{v}) = -\frac{\mathrm{j}\beta\omega_\mathrm{a}}{\rho_0^2 c_0^4}p_{1,\mathrm{tr}}(\mathbf{r}_\mathrm{v})p_{2,\mathrm{tr}}^*(\mathbf{r}_\mathrm{v}), \quad z_\mathrm{v} > 0. \tag{15}$$

C. Insertion loss of the partition

The insertion loss (IL) of the partition for audio sounds generated by the PAL is defined as the difference of the sound pressure level (SPL) at a receiver location $\mathbf{r}$ on the transmission side without and with the partition,

$$L_\mathrm{a}(\mathbf{r}) = 20\mathrm{lg}\left(\left|\frac{p_{\mathrm{a},0}(\mathbf{r})}{p_{\mathrm{a,tot}}(\mathbf{r})}\right|\right)(\mathrm{dB}), \quad z > 0, \tag{16}$$

where $\lg(\cdot)$ represents the common logarithm with the base of 10. In Eq. (16), $p_{\mathrm{a},0}(\mathbf{r})$ is the sound pressure at $\mathbf{r}$ without the partition and can be obtained by changing the upper limit of the integral with respect to the coordinate z_v in Eq. (3) from 0 into the positive infinity.

For comparison, the insertion loss of the partition for a plane wave with the normal incidence (L_n), for a spherical wave from a point monopole (L_m), and for a directional incident sound from a directional end-fire array source consisting of five point monopoles used in Ref. 23 (L_d) are calculated with Eqs. (17), (18), and (19), respectively,

$$L_\mathrm{p} = 20\mathrm{lg}\left(\left|\frac{-\mathrm{j}\omega_\mathrm{a}M + 2\rho_0\omega_\mathrm{a}/k_{\mathrm{a},z}}{2\rho_0\omega_\mathrm{a}/k_{\mathrm{a},z}}\right|\right)(\mathrm{dB}), \tag{17}$$

$$L_\mathrm{m}(\mathbf{r}) = 20\mathrm{lg}\left(\left|\frac{d_\mathrm{m}^{-1}\mathrm{e}^{-\alpha_\mathrm{a}d_\mathrm{m}}}{K(\mathbf{r},\mathbf{r}_\mathrm{m})}\right|\right)(\mathrm{dB}), \quad z > 0, \tag{18}$$

$$L_\mathrm{d}(\mathbf{r}) = 20\mathrm{lg}\left(\left|\frac{\sum_{s=1}^{5} Q_s d_s^{-1}\mathrm{e}^{-\alpha_\mathrm{a}d_s+\mathrm{j}k_\mathrm{a}d_s}}{\sum_{s=1}^{5} Q_s K(\mathbf{r},\mathbf{r}_s)}\right|\right)(\mathrm{dB}), \quad z > 0, \tag{19}$$

where $d_\mathrm{m} = \sqrt{(x-x_\mathrm{m})^2+(y-y_\mathrm{m})^2+(z-z_\mathrm{m})^2}$ is the distance between field point $\mathbf{r}$ and the location of the point monopole $\mathbf{r}_\mathrm{m}$ and $d_s = \sqrt{(x-x_s)^2+(y-y_s)^2+(z-z_s)^2}$ is the distance between $\mathbf{r}$ and the location of the sth point monopole of the end-fire array at $\mathbf{r}_s = (x_s, y_s, z_s)$ with the volume velocity of Q_s.

III. SIMULATIONS AND DISCUSSIONS

In the following simulations, a circular piston with a radius of $a = 0.1$ m is driven with a surface vibration velocity amplitude of 0.12 m/s so that the SPL of both ultrasounds is approximately 125 dB at 1 m away on the axis when the PAL is placed in the free field. The lower ultrasound frequency is set as $f_2 = 60$ kHz. The ultrasound attenuation coefficient in air is 0.228 Neper/m, which is calculated according to ISO 9613-1 at 20 °C, with a relative humidity of 50% at standard atmospheric pressure.[24] The Rayleigh distance at 60 kHz is 5.5 m and the absorption length is 2.17 m. Two kinds of materials are used as the thin partition in the simulations. The first one is aluminum foil with a thickness of 50 μm and a bulk density of 2.7×10^3 kg/m^3. The second one is a polyester fiber blanket with a thickness of 1 mm, a bulk density of 20 kg/m^3, and a flow resistivity of 2000 Pa·s/m^2 (Table I in Ref. 25).

In the calculation, the infinitely large integral domain of the integral in Eqs. (9) and (14) needs to be reduced to a specific region covering the major energy of ultrasound beams, so the integral domain is reduced to a cylindrical column centered in the axis of the PAL with a radius of 3 m (30 times of the PAL radius). The expression for the transmitted audio sounds generated by incident ultrasounds is shown in Eq. (9), and contains a fourfold integral which is time-consuming for calculating the off-axis field. Because $K(\mathbf{r},\mathbf{r}_\mathrm{v})$ depends only on the transverse distance (ρ_v) and longitudinal distance ($|z - z_\mathrm{v}|$) between the two points, it can be precalculated at every transverse and longitudinal distance pairs and then substituted into Eq. (9) to simplify the integral into a threefold one if the frequency and the thickness of the partition are specified.

Figure 2 compares the audio sounds radiated by a PAL, a point monopole and a traditional directional source

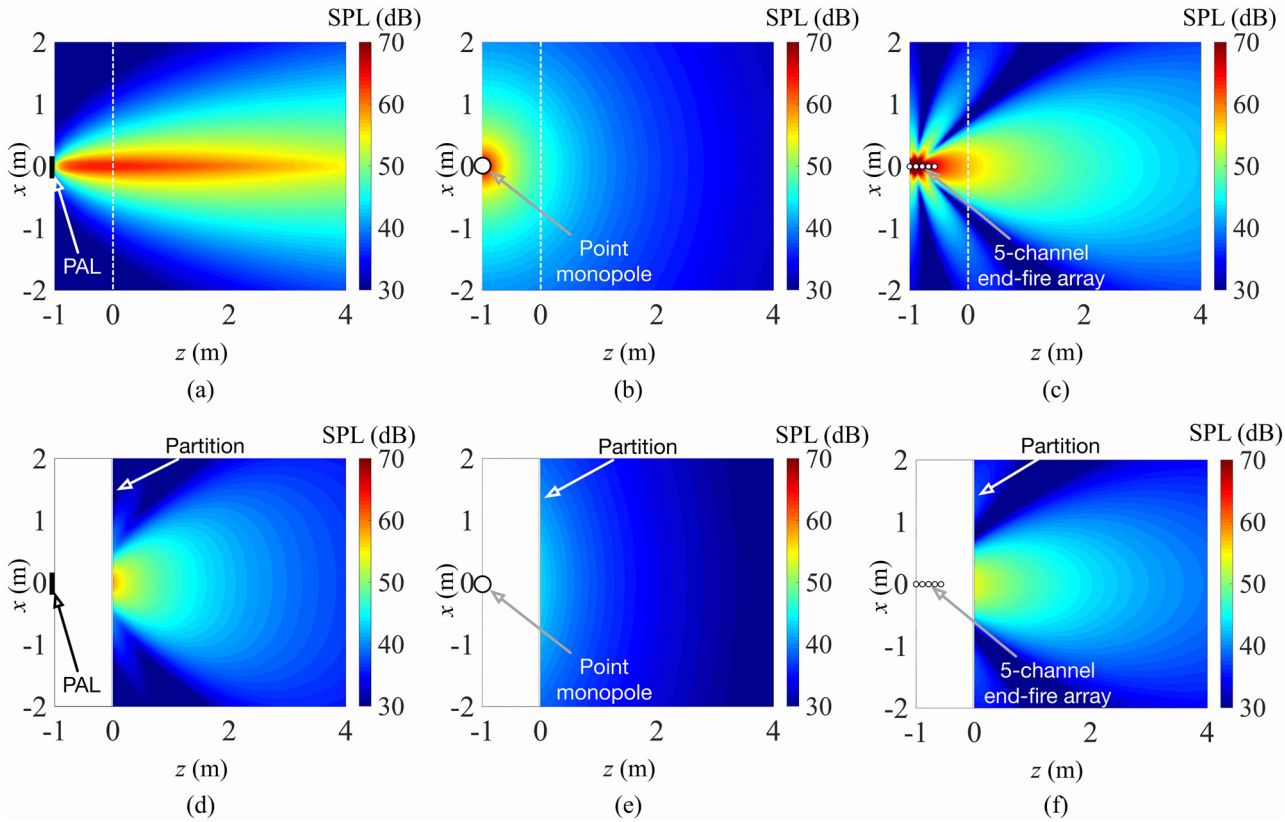

FIG. 2. (Color online) Audio sound fields at $f_a = 1$ kHz with a 50 μm thick aluminum partition and a source at $z_P = -1$ m without the partition for the: (a) PAL, (b) point monopole, (c) end-fire array, and with the partition for the (d) PAL, (e) point monopole, (f) end-fire array.

(5-channel end-fire array[23]) at $f_a = 1$ kHz with and without the aluminum partition. The source is located at $z_P = -1$ m. Figures 2(a), 2(b), and 2(c) show the original sound fields of the sources without the partition, while Figs. 2(d), 2(e), and 2(f) show the total sound fields of the sources with the partition where the sound fields on the incident side are not plotted to focus on the sound transmission. Figures 2(a) and 2(d) are for the PAL, Figs. 2(b) and 2(e) are for the point monopole, and Figs. 2(c) and 2(f) are for the end-fire array. It can be found that the pattern of the sound field generated by a PAL changes significantly behind the partition. The audio sound becomes less focused on the radiation axis, showing a deteriorated directivity. However, the pattern of sound fields radiated by a point monopole or an end-fire array only change slightly behind the partition. The reason is that the directional audio sounds radiated by the PAL is generated by ultrasounds which are almost blocked by the partition, while the aluminum foil is almost transparent for audio sounds radiated by traditional sound sources.

Figure 3 shows the IL along the radiation axis ($x = 0$) on the transmission side ($z > 0$) with different kinds of sources. The IL for the ultrasounds is about 35.7 dB, so the audio sound generated by the transmitted ultrasounds decreases by about 71.4 dB (as the magnitude of the sound pressure of audio sounds is approximately proportional to the square of the magnitude of the one of ultrasounds) and can be neglected. The IL for the traditional sources (the plane wave, the point monopole, or the end-fire array) is about 3.2 dB while the IL of the audio sound generated by the PAL behind the partition can be greater than 17 dB.

The audio sound generated by the PAL behind the partition consists of the transmitted sound of the audio sound generated by incident ultrasounds and the audio sound

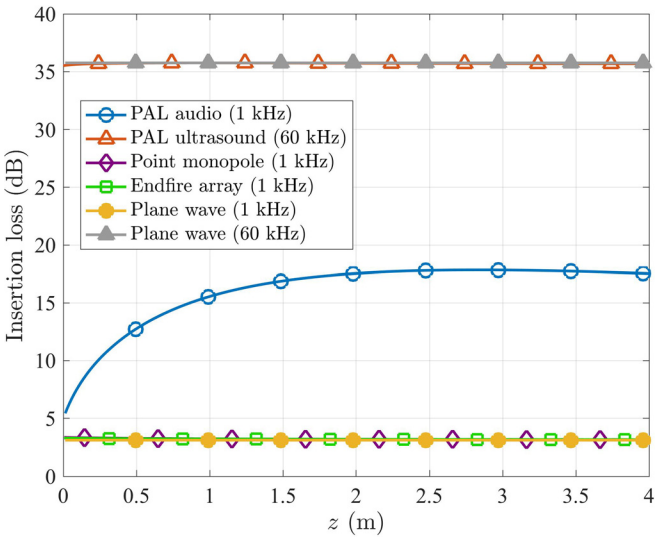

FIG. 3. (Color online) Insertion loss of sounds radiated by different sources through an aluminum partition with a thickness of 50 μm.

https://doi.org/10.1121/10.0001568

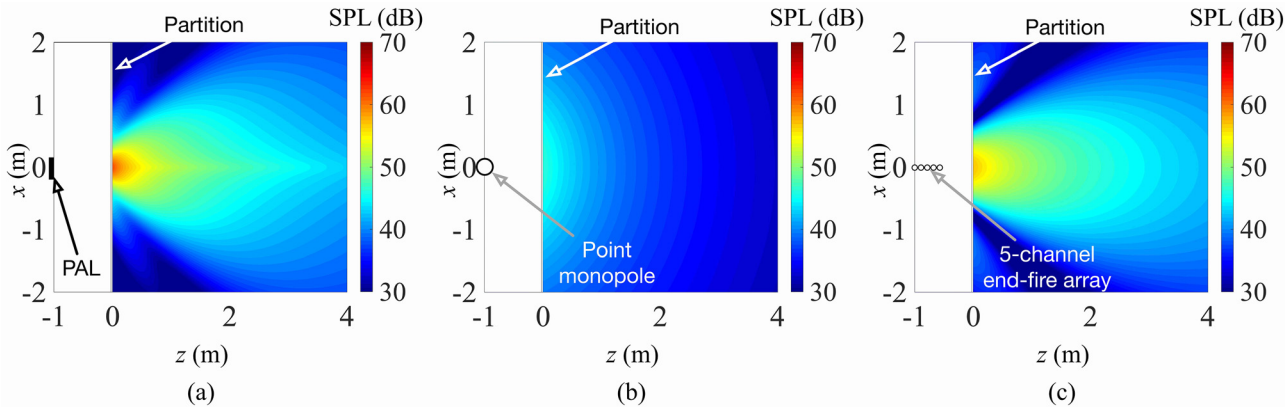

FIG. 4. (Color online) Audio sound field at $f_a = 1$ kHz with a 1 mm thick polyester fibre blanket partition and a source at $z_P = -1$ m: (a) for a PAL; (b) for a point monopole; (c) an end-fire array.

generated by transmitted ultrasounds. Since most ultrasound is blocked by the partition, audio sounds generated by the transmitted ultrasounds are negligible, and the audio sound field behind the partition is dominated by the transmitted sound of the audio sound generated by incident ultrasounds. Large IL (17 dB) for the PAL instead of the small IL (3.2 dB) for the traditional source is observed. The effects of the partition on the transmission of the audio sounds generated by a PAL and traditional sources is completely different and the transmission of ultrasounds should be taken into account for a PAL.

Figure 4 shows the audio sounds radiated by different sources behind a partition made of polyester fiber blanket with a thickness of 1 mm for the sources at $z_P = -1$ m. For a PAL source, audio sounds behind the partition are still focused near the radiation axis which is different from the partition made of aluminum. This is because the IL of the polyester fiber blanket is not sufficiently large for the ultrasounds and some ultrasounds can transmit through the partition to form the directivity of audio sounds. This is demonstrated in Fig. 5, where the IL of the blanket at 60 kHz is only about 10 dB. Figure 4 also illustrates that almost all the sounds transmit through the partition for the traditional sound sources because the ILs are almost 0 as shown in Fig. 5. However, most of the audio sounds radiated by a PAL are blocked by the partition and the IL is approximately 15 dB.

Based on the above findings, the effects of the partition thickness on the amplitude and shape of transmitted audio waves can be discussed. For a traditional loudspeaker, the insertion loss of a thin partition generally increases by 6 dB when the thickness or the frequency is doubled in the mass law frequency range, so for a wide band audio signal, both the amplitude and shape of the transmitted signal changes; however, for a tonal signal, the audio beam shape behind the partition changes a little as the thickness changes. For a PAL, if the transmitted audio sound is mainly generated by the transmitted ultrasonic waves, for example, when the partition thickness is smaller than the ultrasonic wavelength, the insertion loss of the partition increases significantly for the ultrasonic waves as the thickness increases, so the transmitted audio waves becomes smaller and less focused due to the reduced ultrasonic waves. If the transmitted audio sound is mainly generated by the audio waves generated by the ultrasonic waves on the source side, for example, when the thickness is larger than the ultrasonic wavelength, the effects of the partition thickness are similar to that for a traditional loudspeaker.

IV. EXPERIMENTS

The experiments were conducted in a semi-anechoic room with dimensions of 7.20 m × 5.19 m × 6.77 m (height). The sketch and photographs of experimental setups are shown in Fig. 6. The sound fields generated by a PAL, a traditional loudspeaker (point monopole), and a horn loudspeaker (directional source) without and with a partition (a sheet of aluminum foil or a cotton sheet) were measured in the experiments.

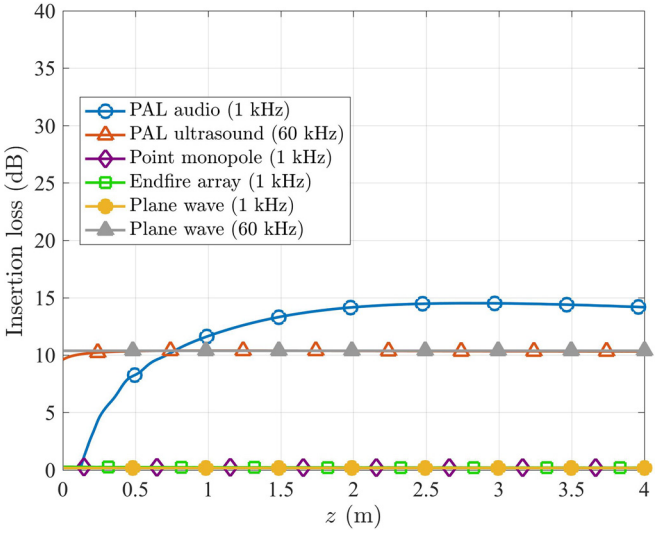

FIG. 5. (Color online) Insertion loss of sounds radiated by different sources through a polyester fiber blanket partition with a thickness of 1 mm.

The sound field was measured at a rectangular grid with $60 \times 41 = 2460$ points and $60 \times 31 = 1860$ points in the xOz plane for the cases without and with the partition, respectively. In all cases, 60 microphones were located in the x direction from $x = -1.45$ m to $x = 1.5$ m with a spacing of 5 cm and they were measured simultaneously with a customary made 60-channel microphone array shown in Fig. 6(b). All measurement microphones were Brüel & Kjær type 4957 calibrated by the Brüel & Kjær 4231 calibrator and the sound pressure at microphones was sampled with a Brüel & Kjær PULSE system (the analyzer 3053-B-120 with the front panel UA-2107-120). The fast Fourier transform (FFT) analyzer in PULSE LabShop was used to obtain the FFT spectrum. For the cases without the partition, the microphone array was located at 41 different positions in the z direction from $z = -1$ m to $z = 3$ m with the spacing being 10 cm. For the cases with the partition, it was located at 31 positions in the z direction from $z = 0$ to $z = 3$ m with the same spacing being 10 cm. In all the measurements, the height of the center of loudspeakers and the microphones is 1.9 m.

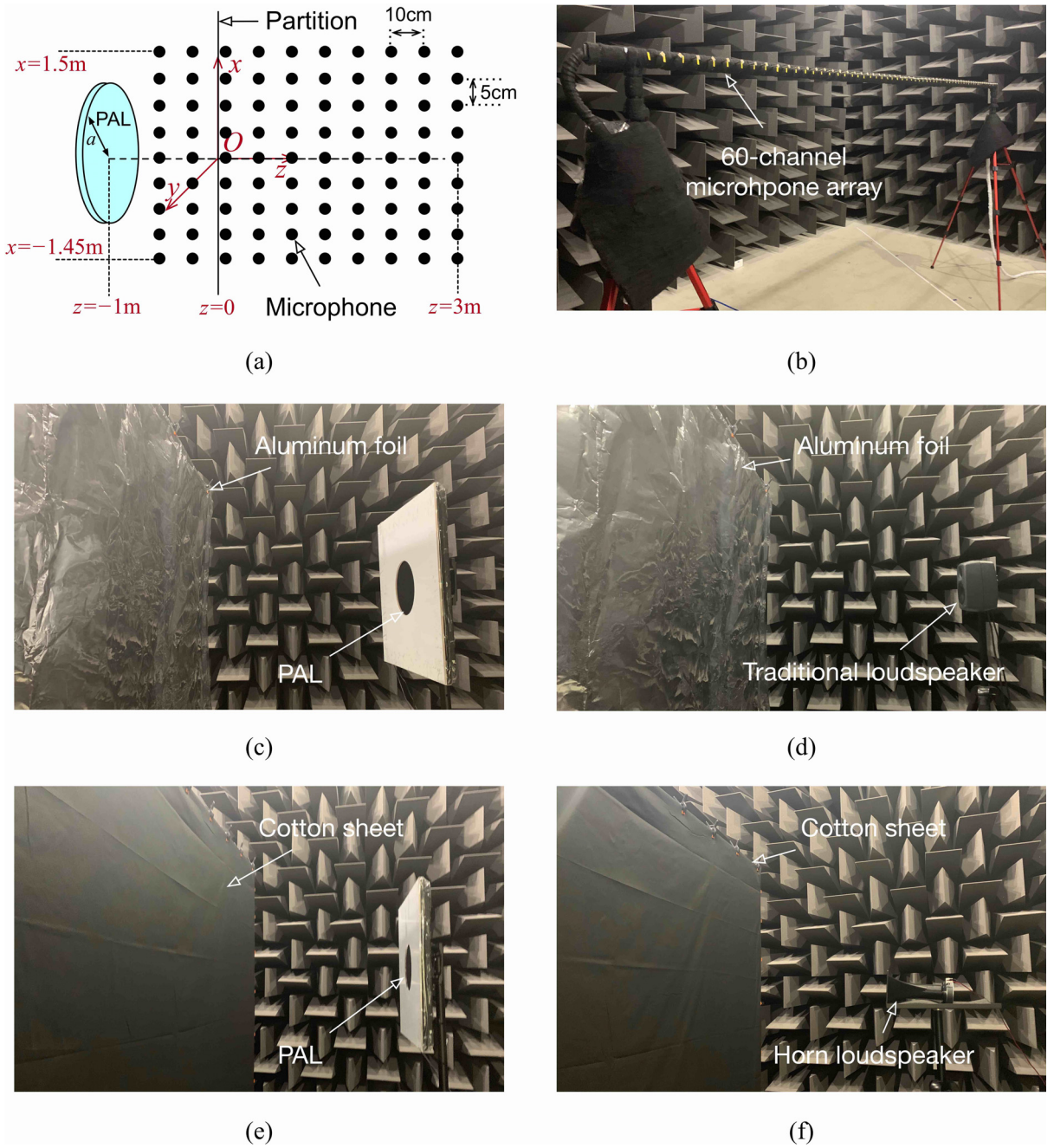

FIG. 6. (a) (Color online) Sketch of the experimental setups; a photo of (b) a 60-channel microphone array; (c) the PAL and the aluminum foil; (d) the traditional loudspeaker (point monopole) and the aluminum foil; (e) the PAL and the cotton sheet; (f) the horn loudspeaker (traditional directional source) and the cotton sheet.

https://doi.org/10.1121/10.0001568

The PAL, the point monopole, and the traditional directional source in the experiments were a Holosonics Audio Spotlight AS-24i with the surface size of 60 cm × 60 cm, a Genelec 8010A traditional voice coil loudspeaker, and a Daichi dome horn loudspeaker with a 24 cm × 8 cm rectangular opening, respectively. The carrier frequency of the PAL is 64 kHz according to the measurements with a Brüel & Kjær type 4939 microphone and the audio frequency in the experiments was set to 1 kHz. The radiating surface of the PAL was covered by a 6 mm thick Perspex panel with a hole of 10 cm radius at the center to construct a circular piston source as shown in Fig. 6(c).

Further experiment results (not presented in this paper) show that the SPLs on the radiation axis of the PAL decrease by more than 30 dB at 1 kHz when the PAL is covered by a same size square Perspex panel, so the panel can provide sufficient IL for audio sounds at 1 kHz, which makes the PAL covered by the panel with a hole a circular piston. To avoid the spurious sounds at microphones induced by the intensive ultrasounds radiated by the PAL,[26] all the microphones are covered by a piece of small and thin plastic film. The experimental results (not presented in this paper) show the insertion loss of this plastic film is more than 30 dB at 64 kHz, which is sufficient for blocking the ultrasonic sounds, and less than 0.6 dB at 1 kHz, which is negligible for the audio sound under tests.

Two partitions were used in the experiments which are a sheet of 50 μm thick aluminum foil with a bulk density of 2.7×10^3 kg/m^3 and a 250 μm thick cotton sheet with a surface density of 0.12 kg/m^2. The size of the aluminum foil and the cotton sheet are 3.6 m (x direction) × 3 m (y direction) and 4 m (x direction) × 2.9 m (y direction), respectively. The center of the loudspeaker is at the same height as that of the aluminum foil or the cotton sheet shown in Figs. 6(c)–6(f). The relative humidity and the temperature in the experiments were 68% and 25.4 °C, respectively.

Figure 7 shows the simulation and experimental results of audio sound fields at 1 kHz generated by the three different sound sources which are at 1.9 m high above ground without partitions. The experimental results of sound fields generated by the PAL with and without the partition are generally in accordance with the predicted ones shown in Figs. 7(a) and 7(d). It can be found the measured sound field radiated by the PAL is highly focused on the radiation axis as expected. Some small fluctuations occur in the z-axis direction in experimental results which might be caused by reflections of the ground. The measured sound fields generated by traditional loudspeakers shown in Figs. 7(b) and 7(c) and 7(e) and 7(f) also agree well with the simulation ones. Figure 7(b) is obtained by using the analytical solution of a point monopole above a rigid ground, and Fig. 7(c) is obtained by the boundary element method solver of the commercial software Virtual.Lab Acoustics.

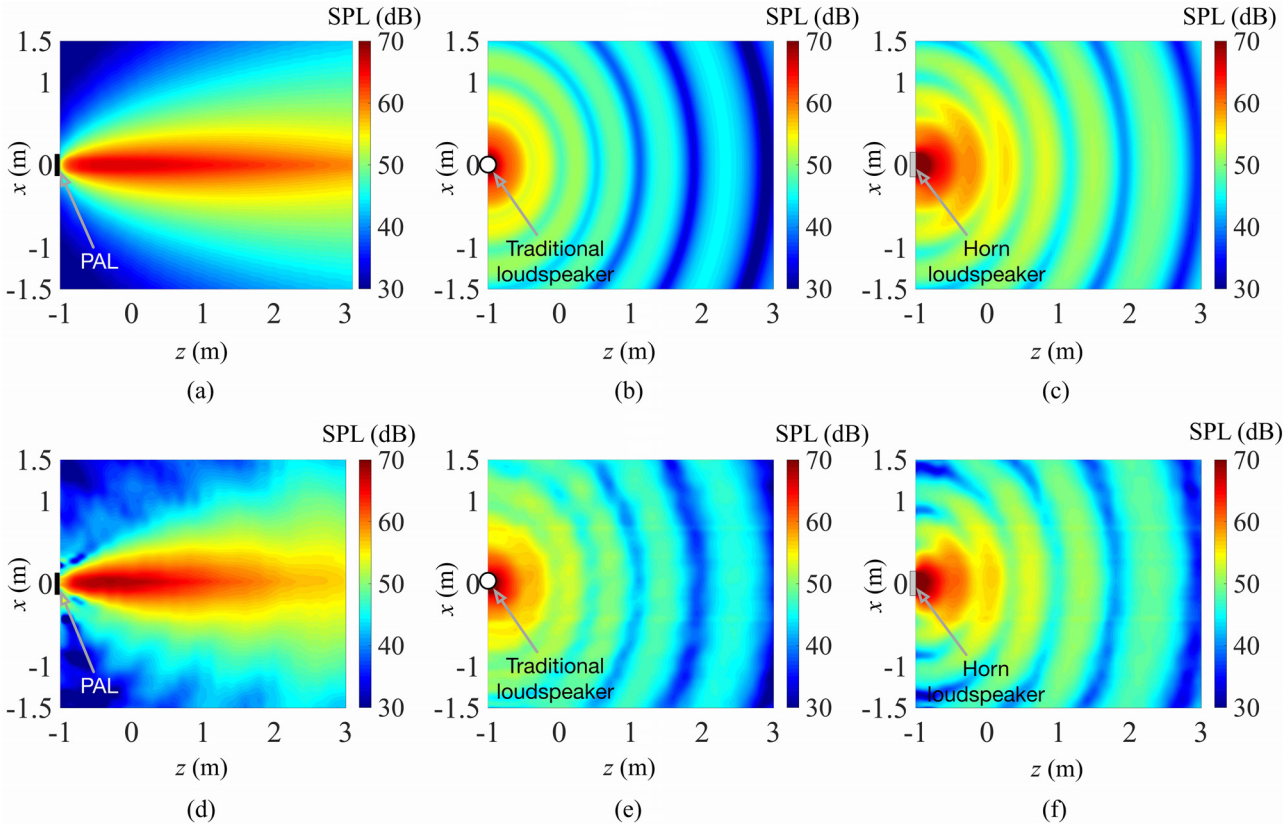

FIG. 7. (Color online) Sound fields at 1 kHz with different sound sources at $z = -1$ m and $x = 0$ above the ground with a height of 1.9 m in the simulations: (a) the PAL, (b) the traditional loudspeaker, and (c) the horn loudspeaker, and in the experiments: (d) the PAL, (e) the traditional loudspeaker, and (f) the horn loudspeaker.

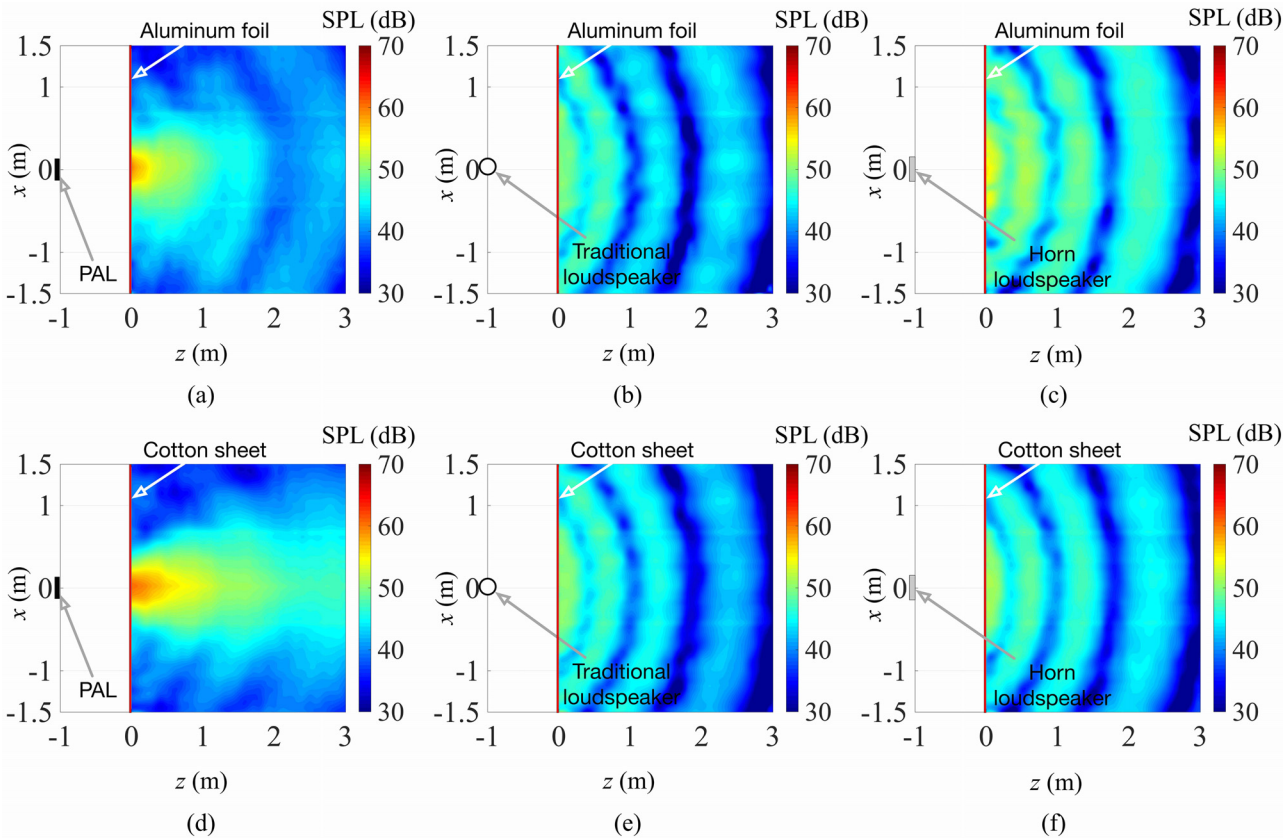

FIG. 8. (Color online) Experimental results of the sound fields at 1 kHz with different sound sources at $z = -1$ m and $x = 0$ above the ground with a height of 1.9 m with a sheet of aluminum foil for (a) the PAL, (b) the traditional loudspeaker, and (c) the horn loudspeaker, and with a cotton sheet for (d) the PAL, (e) the traditional loudspeaker, and (f) the horn loudspeaker.

Figure 8 shows the experimental results of audio sounds at 1 kHz generated by the three sound sources above the ground with a sheet of aluminum foil and a cotton sheet. The sound fields between the loudspeaker ($z = -1$ m) and the partition ($z = 0$) were not measured because they are not the focus point of this paper and also difficult to measure in practice. The theoretical prediction results corresponding to Figs. 8(a) and 8(d) are presented in Figs. 9(a) and 9(b), respectively, where reasonable agreements between predictions and experiments are observed. The small error might be caused by the unevenness of the partition surface in the experiments. It can be found in Fig. 8 that the effects of the thin partitions on the sound transmission loss are small for both the traditional loudspeaker and the horn loudspeaker,

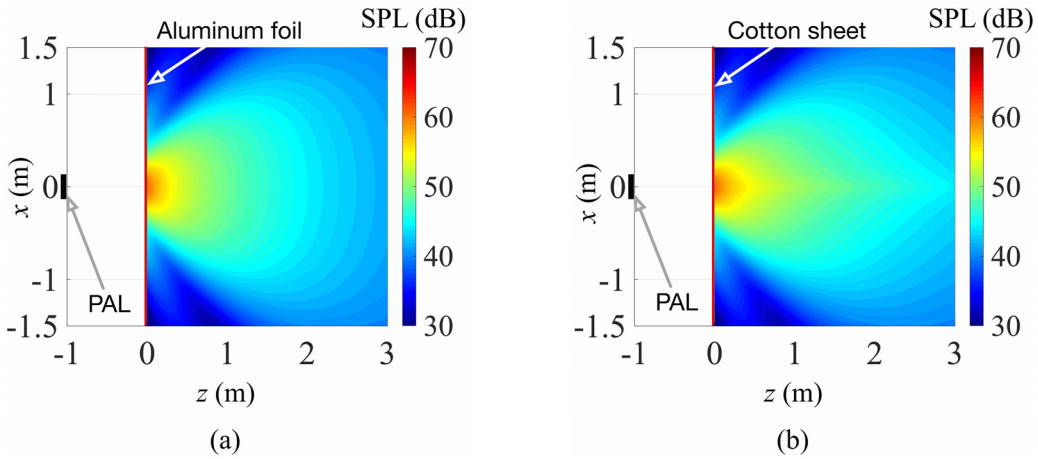

FIG. 9. (Color online) Theoretical prediction results corresponding to Figs. 8(a) and 8(d), i.e., the sound fields at 1 kHz with the PAL at $z = -1$ m and $x = 0$ with (a) a sheet of aluminum foil and (b) a cotton sheet.

but the SPLs generated by a PAL are significantly decreased by the partitions, and audio sounds are less focused on the radiation axis behind the partition because most of the ultrasounds are blocked by the partition. The experiment results support analyses and conclusions in the simulations.

V. CONCLUSIONS

The non-paraxial PAL model and the plane wave expansion method are used under the quasi-linear assumption in this paper to investigate the effects of a thin partition on the propagation of the audio sounds generated by a PAL. Both simulation and experiment results demonstrate that the transmission of audio sounds generated by a PAL through a thin partition is small and less focused on the radiation axis, which is different from that radiated by a point monopole or a traditional directional source. The audio sounds generated by a PAL are significantly blocked by a thin partition due to the large insertion loss of the partitions for ultrasounds. This conclusion makes it possible for constructing an arbitrary shaped PAL from a square/rectangular one by covering it with thin panels. It is also suggested that to apply PALS on mobile phones, more electric power should be provided than expected if it is installed under the screen as the screen can block large amounts of the audio sounds generated by PALS even if it is very thin. Further research includes applying the discoveries in this paper in applications and investigating the reflection of the audio sounds generated by PALS.

ACKNOWLEDGMENTS

This research is supported under the Australian Research Council's Linkage Project funding scheme (LP160100616).

[1]P. J. Westervelt, "Parametric acoustic array," J. Acoust. Soc. Am. **35**(4), 535–537 (1963).
[2]M. B. Bennett and D. T. Blackstock, "Parametric array in air," J. Acoust. Soc. Am. **57**(3), 562–568 (1975).
[3]W. S. Gan, J. Yang, and T. Kamakura, "A review of parametric acoustic array in air," Appl. Acoust. **73**(12), 1211–1219 (2012).
[4]B. Castagnède, A. Moussatov, D. Lafarge, and M. Saeid, "Low frequency *in situ* metrology of absorption and dispersion of sound absorbing porous materials based on high power ultrasonic non-linearly demodulated waves," Appl. Acoust. **69**(7), 634–648 (2008).
[5]H. Ahn, K. Been, I.-D. Kim, C. H. Lee, and W. Moon, "A critical step to using a parametric array loudspeaker in mobile devices," Sensors **19**(20), 4449 (2019).
[6]A. D. Pierce, *Acoustics: An Introduction to Its Physical Principles and Applications* (Springer Nature, Switzerland, 2019).
[7]X. Shi, J. Tao, and X. Qiu, "Sound insulation of an infinite partition subject to a point source incidence," Acta Acust. **33**(3), 268–274 (2008) (in Chinese).
[8]A. Pellicier and N. Trompette, "A review of analytical methods, based on the wave approach, to compute partitions transmission loss," Appl. Acoust. **68**(10), 1192–1212 (2007).
[9]M. F. Hamilton and D. T. Blackstock, *Nonlinear Acoustics* (Acoustical Society of America, New York, 2008).
[10]M. Červenka and M. Bednařík, "Non-paraxial model for a parametric acoustic array," J. Acoust. Soc. Am. **134**(2), 933–938 (2013).
[11]J. Zhong, R. Kirby, and X. Qiu, "A non-paraxial model for the audio sound behind a non-baffled parametric array loudspeaker (L)," J. Acoust. Soc. Am. **147**(3), 1577–1580 (2020).
[12]J. Zhong, R. Kirby, and X. Qiu, "A spherical expansion for audio sounds generated by a circular parametric array loudspeaker," J. Acoust. Soc. Am. **147**(5), 3502–3510 (2020).
[13]H. E. Bass, L. C. Sutherland, and A. J. Zuckerwar, "Atmospheric absorption of sound: Update," J. Acoust. Soc. Am. **88**(4), 2019–2021 (1990).
[14]H. E. Bass, L. C. Sutherland, A. J. Zuckerwar, D. T. Blackstock, and D. M. Hester, "Atmospheric absorption of sound: Further developments," J. Acoust. Soc. Am. **97**(1), 680–683 (1995).
[15]M. Červenka and M. Bednařík, "A versatile computational approach for the numerical modelling of parametric acoustic array," J. Acoust. Soc. Am. **146**(4), 2163–2169 (2019).
[16]S. I. Aanonsen, T. Barkve, J. N. Tjøtta, and S. Tjøtta, "Distortion and harmonic generation in the nearfield of a finite amplitude sound beam," J. Acoust. Soc. Am. **75**(3), 749–768 (1984).
[17]L. M. Brekhovskikh, *Waves in Layered Media* (Academic, New York, 1980).
[18]E. G. Williams, *Fourier Acoustics: Sound Radiation and Nearfield Acoustical Holography* (Elsevier, New York, 1999).
[19]J. J. Wen and M. A. Breazeale, "A diffraction beam field expressed as the superposition of Gaussian beams," J. Acoust. Soc. Am. **83**(5), 1752–1756 (1988).
[20]D. Huang and M. A. Breazeale, "A Gaussian finite-element method for description of sound diffraction," J. Acoust. Soc. Am. **106**(4), 1771–1781 (1999).
[21]H.-J. Kim, L. W. Schmerr, Jr., and A. Sedov, "Generation of the basis sets for multi-Gaussian ultrasonic beam models—An overview," J. Acoust. Soc. Am. **119**(4), 1971–1978 (2006).
[22]M. Červenka and M. Bednařík, "On the structure of multi-Gaussian beam expansion coefficients," Acta Acust. Acust. **101**(1), 15–23 (2015).
[23]Z. Tu, J. Lu, and X. Qiu, "Robustness of a compact endfire personal audio system against scattering effects (L)," J. Acoust. Soc. Am. **140**(4), 2720–2724 (2016).
[24]ISO 9613-1:1993, "Acoustics—Attenuation of sound during propagation outdoors—Part 1: Calculation of the absorption of sound by the atmosphere" (International Organization for Standardization, Geneva, 1993).
[25]M. Garai and F. Pompoli, "A simple empirical model of polyester fibre materials for acoustical applications," Appl. Acoust. **66**(12), 1383–1398 (2005).
[26]P. Ji and J. Yang, "An experimental investigation about parameters' effects on spurious sound in parametric loudspeaker," Appl. Acoust. **148**, 67–74 (2019).